IAC-22,B1,IP,7,x68955

Reference Mirror Misalignment of Cold Atom Interferometers on Satellite-Based Gravimetry Missions

Jaspar Meister[1,*], Stefanie Bremer[1], Alireza HosseiniArani[2], Andreas Leipner[1], Meike List[1], Jürgen Müller[2], and Manuel Schilling[1]

[1]German Aerospace Center, Institute for Satellite Geodesy and Inertial Sensing, Bremen, Germany
[2]Leibniz University Hannover, Institute for Geodesy, Hannover, Germany

[*]Corresponding author: jaspar.meister@dlr.de

Abstract

The success of GRACE-FO and its predecessors has demonstrated the benefits of satellite gravimetry for monitoring mass variations on the Earth's surface and its interior. However, the demand for increasingly higher spatial and temporal resolution of gravity field solutions has brought into focus the need for next-generation gravimetry missions (NGGMs). Therefore, we investigate the hybridization of electrostatic accelerometers (E-ACC) with cold atom interferometers (CAI), which can reduce the instrumental error contribution of the E-ACC, e.g. by enabling in-flight estimation of E-ACC bias parameters, and reduce systematic effects in gravity field solutions by proving drift free measurements. However, these sensors introduce more stringent requirements on the computation of environmental disturbances in lower Earth orbits, as the alignment of the CAI's reference mirror has to be controlled precisely. Therefore, the movement of the CAI's reference mirror inside the satellite is analyzed using the Hybrid Simulation Platform for Space Systems (HPS) developed by DLR and ZARM (University of Bremen). Misalignments and vibrations of the reference mirror cause an additional CAI phase shift, which introduces measurement inaccuracies. Our work examines the translational displacement, rotational misalignment and angular velocity of the reference mirror, due to forces transferred by the coupling link between mirror and satellite. This helps to compare different hybridization concepts and to improve noise and signal models for CAI accelerometers.

Keywords: accelerometer, simulation, cold atom interferometer

1. Introduction

Satellite gravimetry missions like the Gravity Recovery And Climate Experiment and its Follow-On mission [GRACE and GRACE-FO; 1, 2] provided major insights into climate change driven processes on the Earth and in the oceans [3, 4]. The main improvement from GRACE to its successor mission GRACE-FO is the introduction of a inter satellite laser ranging interferometer as a demonstrator [LRI; 5] in addition to the microwave ranging system, which is still the main instrument. The ranging instrument measures the change of the distance between the two satellites of the pair. The distance between the satellites changes due to the gravity field of the Earth and non-gravitational accelerations, e.g. solar radiation pres-

sure, atmospheric drag, Earth albedo, acting on the satellite. In future satellite gravimetry missions, concepts like the LRI will very likely be the main instrument of the mission. The main contributor to the instrumental error budget of a GRACE-FO type mission is now the electrostatic accelerometer (E-ACC) which measures the non-gravitational forces [see e.g. 6]. These measurements are used to remove the effect of non-gravitational accelerations on the inter satellite distance from the ranging observations. Therefore, accelerometer performance has a direct impact on the recovered gravity field. The current generation of E-ACC are characterized by a drift below 10^{-3} Hz which contributes to the characteristic "striping effect" seen in GRACE(-FO) monthly solutions. Other contributors to this effect are the observation geometry and

temporal aliasing due to unmodeled changes of atmosphere and ocean [7]. In order to meet the needs of the scientific user community of gravity field products [8] the performance of the accelerometer needs to be improved in lower frequencies.

Cold atom interferometer (CAI) based accelerometers offer a lower drift or possibly drift-free performance over a broader bandwidth compared to E-ACC. Numerous studies have shown the benefit to gravity field solutions of combining a CAI- and E-ACC or employing a CAI gradiometer on a satellite gravimetry mission These studies might also include a preliminary design for the CAI instrument [9, 10] but often introduce the CAI instrument as noise based on the assumption of white noise with a certain amplitude in the signal synthesis step of a simulation [see e.g. 11, 12]. In addition to this, methods to combine the CAI and E-ACC into a hybrid accelerometer are investigated [13]. Our study builds upon the work to model the dynamics of an E-ACC test mass in a satellite environment [14] to simulate a hybrid CAI-/E-ACC on a satellite under consideration of external forces acting on the satellite and thus on the instrument.

We model the test mass behavior on a GRACE like satellite, which also acts as reference mirror in a hybrid accelerometer. This includes the variation of position of the test mass within the accelerometer and the acceleration experienced by the test mass, as well as the rotation of the test mass with respect to the satellite and the angular velocity and acceleration of the test mass (section 3). We investigate the effect of a rotating test mass acting as reference mirror and a fixed reference mirror, independent of test mass movements, on the atom interferometer measurement and the necessary control with respect to test mass movement and rotation to be able to benefit from the hybridization (section 4).

2. Cold Atom Interferometry

A cold atom interferometer uses atoms as test masses to measure inertial forces and rotations [15]. On a satellite, an atom interferometer can be used to measure the non-gravitational accelerations, e.g. atmospheric drag, solar radiation pressure, Earth albedo, acting on the satellite. The principle of two photon Raman transitions described by Kasevich and Chu [16] is most commonly applied in, e.g., terrestrial applications like gravimeters and simulation studies on accelerometry in space. However, there are a wide range of different principles using cold atoms. The creation of Bose-Einstein condensates in space has also been demonstrated [17], which is a candidate for

future quantum sensors on a satellite.

A single measurement of the CAI can be divided into three phases: 1) preparation of atoms, 2) free fall and interferometer sequence, 3) detection of atomic states. During the preparation phase the atoms, e.g. Rubidium ^{87}Rb, are cooled down to a few µK and are selected to be in one specific state. The atoms interact with three pulses of counter-propagating laser beams (Raman beams) spaced in a time interval T during the free fall and interferometry phase. The first pulse has a probability of 50 % of an interaction of two photons with one atom, thereby raising the atom into an excited state, putting the atoms in a superposition of initial and excited state. This pulse acts as a beam splitter in the atom interferometer. The second pulse switches the states of all atoms from the excited state back to the initial state or vice versa and is called a mirror pulse. The third pulse is also a beam splitter closing the interferometer. During each interaction between two photons and an atom, the energy and momentum of the absorbed/emitted photons is gained/lost by the atoms. The population of the two atomic states is measured in the detection step of the CAI measurement. The atom interferometer phase shift $\Delta\Phi$ can be calculated from the detected population of a state P_e

$$P_e = \frac{1}{2}\left(1 - \cos\Delta\Phi\right).$$

$\Delta\Phi$ depends on the acceleration $\vec{a}$ the atoms experience during free fall and the effective laser wave vector $\vec{k}_{eff}$

$$\Delta\Phi \approx \vec{k}_{eff} \cdot \vec{a} \cdot T^2. \tag{1}$$

$\vec{k}_{eff}$ is defined as the difference of the two laser wave vectors $\vec{k}_{1,2}$ of the counter-propagating beams: $\vec{k}_{eff} = \vec{k}_1 - \vec{k}_2$. As $\vec{k}_2 \approx -\vec{k}_1$ and considering the reduced Planck constant $\hbar$ the momentum transferred is approximately $2\hbar\vec{k}_1$ [15].

The lasers typically enter the vacuum chamber through a single optical telescope and one of the lasers is reflected by the inertial reference, a retro-reflecting mirror, to be in resonance with the desired atomic transition. The method to model the behavior of this inertial reference will be described in section 3. In our study the lasers are aligned with the along track direction and more details on this will be given in section 4. The measurement of the CAI is therefore the projection of $\vec{a}$ on $\vec{k}_{eff}$, which is the acceleration a in the along track direction. Assuming a perfect orientation of the CAI in the along track direction, Eq. (1) is simplified to $\Delta\Phi \approx k_{eff} \cdot a \cdot T^2$.

The parameters in Eq. (1) to adjust the sensitivity (or increase the phase shift $\Delta\Phi$) are the chosen

method of momentum transfer (changing $\vec{k}_{eff}$) and the time interval T. In terrestrial applications, T is limited by the size of the free fall distance to a few $100\,\mathrm{ms}$ for mobile and about $1\,\mathrm{s}$ in stationary atom interferometers. Applications in space can potentially extend T to several seconds. The limiting factors are, for example, the thermal expansion of the atom cloud or the rotation of the satellite.

The latter results in the rotation of the lasers with respect to the inertial frame during a single interferometer sequence, so the direction of $\vec{k}_{eff}$ is different for the three laser pulses. The compensation for this is achieved by counter rotating the Raman beam vector [18]. The largest rotation for an along track CAI is around the cross track axis with $\approx 1.1\,\mathrm{mrad\,s^{-1}}$ (see also Fig. 1).
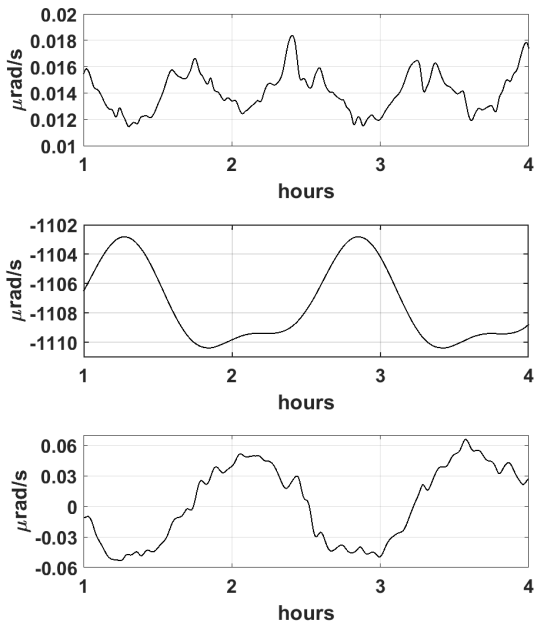

Fig. 1: Angular velocity of the satellite in satellite body frame with X_{Sat}, Y_{Sat} and Z_{Sat} axis (top to bottom).

The gradiometer design given by Migliaccio et al. [10] employs multiple mirrors mounted at specific angles, resulting in three (inertial) parallel laser pulses for a fixed interval T. This design compensates the largest contribution and active tilting of mirrors can be added for small residual rotations. Zahzam et al. [19] describe the use of the E-ACC as reference mirror of the CAI and rotating the E-ACC test mass at specific rates to counter the satellite's rotation. The topic of rotations will be discussed further in section 3 and 4. The impact of changes of a dur-

ing one interferometer sequence is discussed in Knabe et al. [20]. Additionally, the CAI measures a phase shift in the interval $0-2\pi$, resulting in an ambiguity problem, if the change of acceleration a within two successive measurements, translated in atom interferometer phase shift, is larger than 2π. Ideally, the change should be below $\pi/2$ as it can also not be distinguished between the rising and falling slope of the atom interferometer fringe [for details on our solution see 13].

3. Test Mass Modeling

The first application of the test mass dynamics modeling is a CAI sensor concept, where the laser beams are reflected directly by the surface of the test mass. Translational and rotational movement of the test mass are not specifically controlled to improve CAI performance, but are allowed to occur based on satellite - test mass coupling to investigate the effect on the CAI measurement.

3.1 Simulation Scenario

This study uses several frames, which are depicted in Fig. 2. The Earth centered inertial (ECI) frame is used for the satellite orbit integration. The satellite body frame with X_{Sat} in the along track, Y_{Sat} in the cross track and Z_{Sat} in the radial direction is identical to the GRACE-FO Satellite Frame [21]. The accelerometer frame is rotated with respect to the body frame, so the Z_{ACC} axis points in the along track and X_{ACC} in the cross track direction.
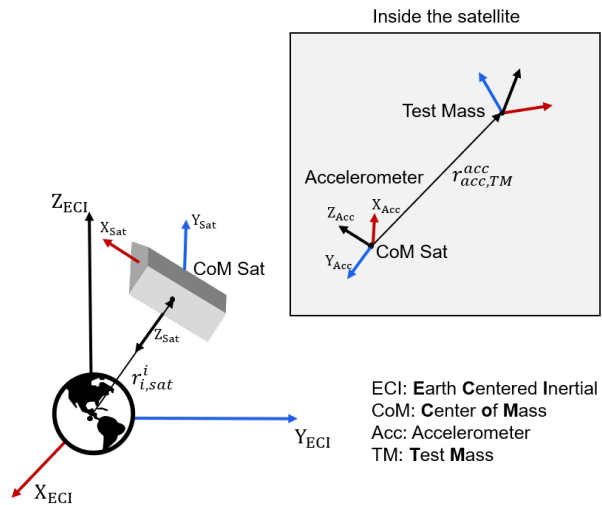

Fig. 2: Overview of frames used in this work.

The origin of the satellite frame is in the center of mass (CoM) of the satellite [21]. Under ideal cir-

cumstances, the test mass CoM coincides with the satellite CoM. However, it is possible to apply an offset to the origin of the accelerometer frame, to study the effect of small deviations from the CoM.

We simulate an E-ACC on a GRACE-FO type satellite in the Hybrid Simulation Platform for Space Systems [22]. The accelerometer's parameters are taken from [21] to closely resemble the GRACE-FO mission. The initial conditions of the orbit simulation are taken from GRACE-FO data products of 01.02.2020 0:00.

The simulation scenario includes several non-gravitational forces, which act on the satellite. Solar radiation, albedo, Earth infrared and thermal radiation pressure are modeled using a finite element model of the satellite to determine illumination and shadowing conditions with respect to the satellite's attitude. Absorption and emission coefficients characterize each surface of the satellite, with values taken from [21]. The simulation incorporates the atmospheric density model JB2008 developed by Bowman et al. [23] and uses a constant drag coefficient of 2.4 [24]. To model the test mass, it is assumed that the test mass is properly shielded from direct environmental effects acting on the satellite, only gravitational forces, control forces and coupling forces from the satellite act on the test mass. The coupling forces describe the connection between test mass and satellite. They are centering the test mass inside the satellite and keep it from escaping. A mass-spring-damper model describes the link between test mass and satellite. This link thus transfers the non-gravitational forces to the test mass. By adjusting the spring and damping coefficient matrices, the individual behavior of the link is set.

In principle, the test mass equations of motion can be derived in the accelerometer frame as well as in the inertial frame. However, if implementing the equations of motion for the test mass in the inertial frame numerically, difficulties may arise if high accuracy for the small displacements between satellite and test mass has to be achieved. Therefore, the test mass is described in the accelerometer frame [see Fig. 2 and 14]. The test mass states consist of the angular velocity, attitude quaternions, position and velocity. To derive the states, the acceleration of the test mass has to be determined, which can be split in a translational and rotational part.

The translational acceleration $\vec{a}_{trans}^{ACC}$ acting on test masses in the accelerometer frame is given by

$$\vec{a}_{trans}^{ACC} \;=\; \vec{a}_{gg}^{ACC} + \vec{a}_{coup}^{ACC} + \vec{a}_{rot}^{ACC}. \qquad (2)$$

It consists of gravitational $\vec{a}_{gg}^{ACC}$ and coupling $\vec{a}_{coup}^{ACC}$ acceleration, which are the main contributors to the translational acceleration. Furthermore, there is translational movement of the test mass due to the rotation of the satellite $\vec{a}_{rot}^{ACC}$. However, as the satellite's attitude is controlled, the resulting acceleration is small.

Acceleration due to Satellite Test Mass Coupling: A mass-spring-damper model is applied to calculate the link forces and torques between test masses and satellite. The coupling acceleration for the test mass is computed as follows:

$$\vec{a}_{coup}^{ACC} \;=\; \frac{\vec{F}_{dc,trans} - \vec{F}_s - \vec{F}_d}{m_{tm}} \quad .$$

The coupling force consists of the spring $\vec{F}_s$ and damping $\vec{F}_d$ forces as well as a control force $\vec{F}_{dc,trans}$. The link can be characterized via stiffness and damping matrices, spring offsets, constant link forces and torques.

Gravitational Acceleration: The calculation of the gravitational acceleration applies the expansion of spherical field to avoid differences of large numbers. The algorithm is based on an expansion of the spherical gravitational field [14]. The calculation depends on the satellite position $\vec{r}_{i,b}^i$ and the test mass displacement from satellite CoM in inertial frame $\vec{x}^i$.

Acceleration due to Satellite Rotation: The acceleration $\vec{a}_{rot}^{ACC}$ acts on the test masses due to the satellite's rotation (cf. Eq. (2)). It is divided into a Coriolis term $\ddot{\vec{x}}_{coriolis}$, a centrifugal term $\ddot{\vec{x}}_{centrifug}$ and an Euler term $\ddot{\vec{x}}_{newton}$. Thus, the total amount of $\vec{a}_{rot}^{ACC}$ is given by

$$\vec{a}_{rot}^{ACC} \;=\; -2 \cdot \ddot{\vec{x}}_{coriolis} - \ddot{\vec{x}}_{centrifug} - \ddot{\vec{x}}_{newton}.$$

The total amount of angular acceleration $\dot{\vec{\omega}}_{tm}^{ACC}$ can be computed applying the formula,

$$\dot{\vec{\omega}}_{tm}^{ACC} \;=\; \left(\mathbf{I}_{tm}^{ACC} \right)^{-1} \cdot \vec{T}_{tot}^{ACC} \quad ,$$

with the moment of inertia matrix $\mathbf{I}_{tm}^{ACC}$ and the total torque $\vec{T}_{tot}^{ACC}$. It consists of the coupling torque between test mass and satellite, as well as the Euler term

$$\vec{T}_{tot}^{ACC} \;=\; \vec{T}_{coup}^{ACC} - \vec{T}_{euler}^{ACC} \quad .$$

The Euler term $\vec{T}_{euler}^{ACC}$ is computed with

$$\vec{T}_{euler}^{ACC} \;=\; \vec{\omega}_{i,tm}^{ACC} \times \left(\mathbf{I}_{tm}^{ACC} \cdot \vec{\omega}_{i,tm}^{ACC} \right) \quad .$$

The computation of the coupling torques is done in the same way as for the coupling forces. The sum of all torques yield

$$\vec{T}_{coup}^{ACC} = \vec{T}_{dc,rot} - \vec{T}_s - \vec{T}_d.$$

For the CAI analysis, the test mass angular velocity and acceleration have to be transformed from the accelerometer frame to the ECI frame.

3.2 Simulation Results

Figure 3 shows the measurement and model of non-gravitational accelerations in the satellite frame. The test mass acceleration includes not only the non-gravitational acceleration but also the influence of the coupling link, with its characteristics. The test mass is placed at the center of mass of the satellite. The GRACE-FO ACT1B data product [25] is compared to the test mass acceleration simulated in HPS. The satellite simulation does not include any correction burns, thus peaks in the satellite's Y_{Sat} do not appear in the simulation. Jumps in the simulated acceleration data, indicating penumbra transitions into and out of the Earth's shadow, are due to solar radiation pressure and clearly coincide with the measurement data. Especially, the data for X_{Sat} closely follows the measurement data. Thus, the selection of stiffness and damping coefficients chosen for the test mass connection result in reasonable outcomes. Therefore, the following calculations for the translational movement of the test mass are conducted with same link characteristics.
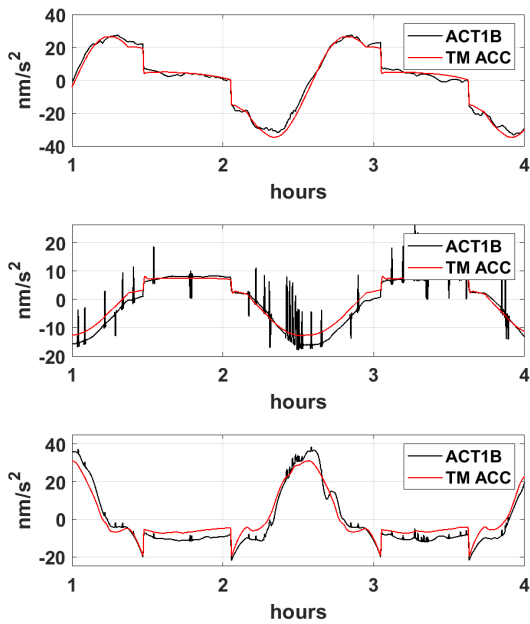

Fig. 3: Accelerometer measurement (ACT1B) and test mass acceleration (TM ACC) for the X_{Sat}, Y_{Sat} and Z_{Sat} axis (top to bottom) with mean removed.

The angular velocity is given in the Earth centered inertial (ECI) frame. As the test mass is not rigidly connected to the satellite, it has its own degrees of freedom. Therefore, it can move inside the satellite, which means that the test mass' angular velocity deviates from the satellite's angular velocity. By setting the rotational link connections between test mass and satellite, the motion is adjusted. Figure 4 shows the difference between the angular velocity of the satellite and test mass, which results from the slightly different acceleration of the test mass compared to the satellite, due to the coupling forces. Relative to the satellite, the test mass is rotating with a few dozen $\mathrm{nrad\,s^{-1}}$. The influence of a rotating mirror on the measurement of the phase shift is investigated further in section 4.
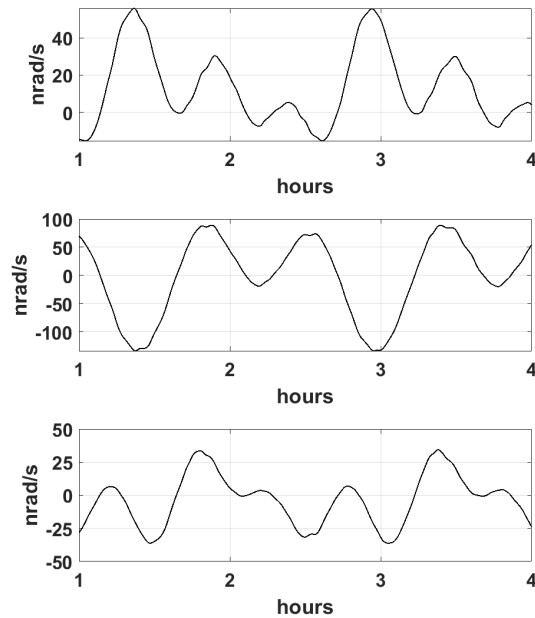

Fig. 4: Difference between angular velocity of test mass and satellite in ECI frame with the X_{ECI}, Y_{ECI} and Z_{ECI} axis (top to bottom).

Due to mass fluctuations of the satellite or for constructional reasons, a certain amount of offset from the accelerometer origin to the satellite CoM has to be accounted for. Therefore, the accelerometer frame of the test mass is moved $0.15\,\mathrm{mm}$ in Z_{Sat} away from the center of mass of the satellite. The translational link between test mass and satellite is set to let the test mass move freely in the range of a few micrometers. Figure 5 shows the test mass position inside the satellite depicted in the accelerometer frame.
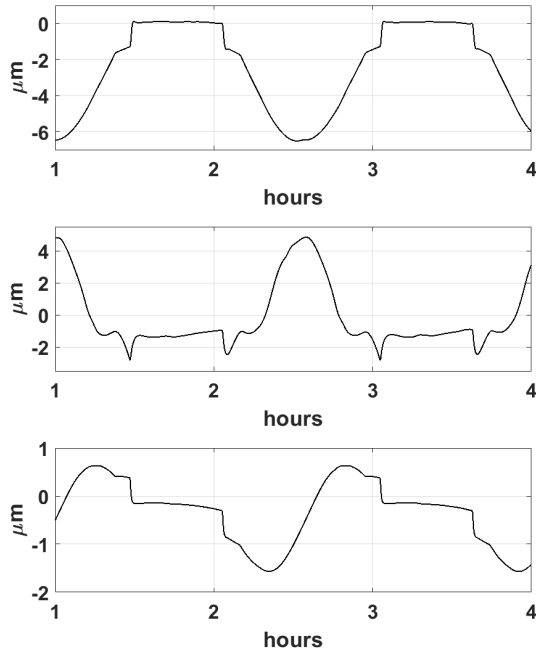
Fig. 5: Position of test mass in the accelerometer frame with the X_{ACC}, Y_{ACC} and Z_{ACC} axis (top to bottom).

4. CAI Modeling

Details on the modeling of the hybrid accelerometer by combining a CAI- and E-ACC are given in [13]. In this study, we assume a CAI with a white noise behavior at a level of $10^{-10}\,\mathrm{m/s^2}/\sqrt{\mathrm{Hz}}$. Previous studies [e.g. 12] have shown no benefit for the gravity field recovery by introducing a CAI-ACC with a lower performance in a hybrid ACC. The white noise assumption, at least at this level of performance, is based on currently available terrestrial instruments and long term measurements [e.g. 26]. Possible low frequency drifts, comparable to the behavior of E-ACC, would depend to a great extent on the frequency stability of the laser system. Laser frequency stabilization is also of high interest for future iterations of the LRI system on next generation gravity field missions [27], so a CAI also benefits from current lessons learned of the GRACE-FO mission [5, 28].

In the following, we focus on the implementation of rotational components of the reference mirror/test mass of the E-ACC. The attitude and orbit control system of GRACE-FO is able to control the attitude of the satellite to within $\pm 100\,\mu\mathrm{rad}$ [29], which is the technical requirement for operating the LRI. Further improvements in attitude determination can be achieved by combining differential wavefront sensing and attitude measurements from the fast steering mirror of the LRI with conventional sensors (star camera and IMU). The accuracy with which the angular ac-

celeration of the test mass in accelerometers currently under development can be determined is estimated to be $\pm 2.2 \times 10^{-10}\,\mathrm{rad\,s^{-2}}$ [30]. Here, we want to estimate the effect of test mass/reference mirror rotation on the CAI-ACC and assume perfect knowledge of satellite and test mass rotations to model this effect. The inclusion of these error estimates is ongoing work and not discussed here in detail. The mirror of CAI accelerometer acts as a reference for its measurements. When it is connected to the test mass, the translational displacement of the test mass, as shown in Fig 5, would cause an atomic phase shift in the CAI accelerometer. This can be calculated by considering the linear acceleration of the test mass (see Fig. 3), as the input acceleration of the CAI accelerometer.
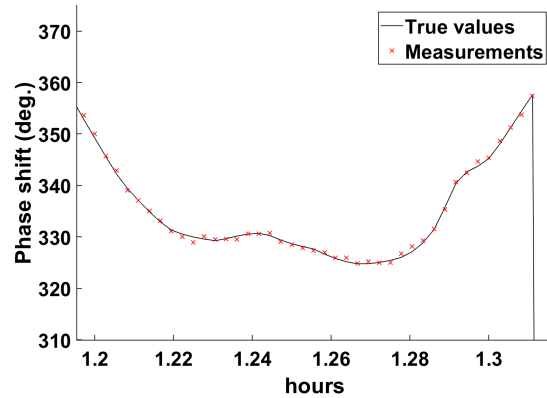
Fig. 6: Black: True values of the phase shift; Red: CAI measurements of the phase shift.
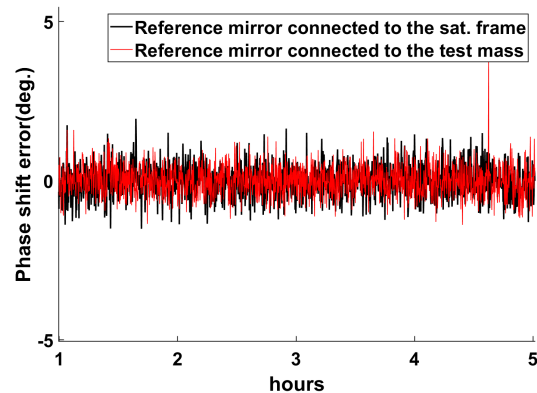
Fig. 7: Error on the measurement of the CAI phase shift because of the translational displacements of the reference mirror; Black: reference mirror is connected rigidly to the satellite body frame; Red: Reference mirror is the test mass.

Figure 6 compares the true values of the CAI phase shift (equivalent to the true non-gravitational forces acting on the satellite) with the measurements of the phase shift based on the displacements of the reference mirror (test mass).

Figure 7 shows the phase shift error because of the translational displacements and vibrations of the reference mirror. It compares two scenarios: In the first scenario, the reference mirror is connected rigidly to the satellite body frame and in the second one, the reference mirror is the test mass. One can notice that there is no meaningful difference in the noise level between the two scenarios. The angular misalignment of the reference mirror is not considered here.

Apart from this phase shift, there is an additional phase shift which comes from the angular velocity of the reference mirror. When the reference mirror is connected to the test mass, the angular velocity of the test mass (see Fig. 4), would cause an additional atomic phase shift in the CAI accelerometer. This can be modeled by considering the linear acceleration of the test mass, as the input acceleration of the CAI accelerometer. This additional phase shift can be calculated adapting the non-vector solution of Eq. (1):

$$\Delta\Phi = k_{eff} \cdot R \cdot \omega_{TM}{}^2 \cdot T^2 + 2 \cdot k_{eff} \cdot \omega_{TM} \cdot V_T \cdot T^2 \quad (3)$$

Where ω_{TM} is the angular velocity of the test mass, R is the distance of the reference mirror to the center of mass and V_T is the transverse velocity of the atomic cloud (perpendicular to the CAI sensitivity axis). The first term of Eq. (3) is the phase shift due to the centrifugal accelerations and the second term is the phase shift due to the Coriolis acceleration. The assumption here is that the angular velocity of the mirror is constant during the interrogation time. For more realistic simulations, we consider Eq. (3) in an integral form.

The main contribution of the rotation on the atom interferometer phase shift comes from the Sagnac effect induced by the transverse velocity of the atomic cloud. Because of the lack of knowledge on the transverse velocity of the atoms and also because of the contrast loss of the atom interferometer, it would not be easy to mathematically compensate for the Coriolis effect. Therefore, physical approaches are needed to overcome this effect. One possible approach explained by Migliaccio et al. [10] is the static compensation for spacecraft rotation in order to cancel Coriolis acceleration. In this approach, mirrors are aligned to form an angle $\Omega_{orb} \cdot T$ between the Raman wave vectors at successive pulses [see Fig. 1-B in 10].
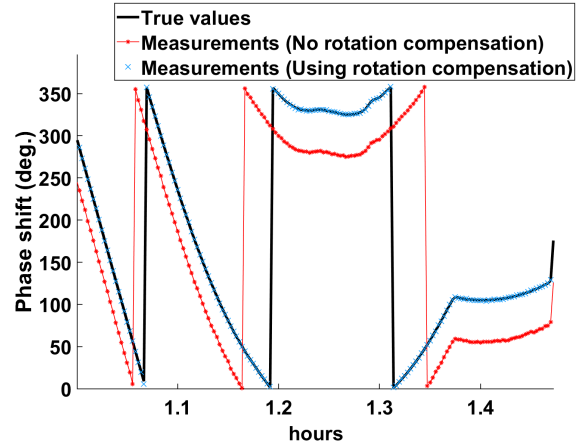

Fig. 8: Black: True values of the phase shift (phase shift equivalent of the true non-gravitational accelerations); Red: CAI measurements of the phase shift based on both the translational displacement and angular velocity of the test mass. No rotation compensation is assumed; Blue: CAI measurements of the phase shift based on both the translational displacement and angular velocity of the test mass using a counter-rotation of the Raman wave-vector.

Figure 8 compares the true values of the CAI phase shift with the measurements of the CAI phase shift based on the translational displacement and angular velocity of the reference mirror (test mass) in two different scenarios: In the first scenario, we assume to have measurements with no physical approach for the compensation of the test mass angular velocity. In the second scenario, we apply a physical rotation compensation approach by assuming a tip-tilt mirror on the test mass. One can notice that the measurements without a physical rotation compensation, suffer from a large bias on the measurements. However, when the counter-rotation of the Raman wave vector is considered, the biases on the measurements disappear and the measurement accuracy improves. In the latest case, the total measurement error is only slightly ($\sim 10\%$ to 20%) higher than the case where we purely considered the translational acceleration of the test mass without including the impact of rotation (Fig. 7).

The measurements of the CAI and the conventional IMUs have different sampling rates, e.g. $0.1\,\mathrm{Hz}$ and $10\,\mathrm{Hz}$, which have to be combined to create a hybrid accelerometer. In this study, we use an extended Kalman filter (EKF) approach [31] for the hybridization of the measurements. This filter uses the measurements of the conventional IMU as input to the dynamic model in order to predict the phase shift of the atom interferometer and it solves for the fringe ambiguity. The CAI measurements is then used as

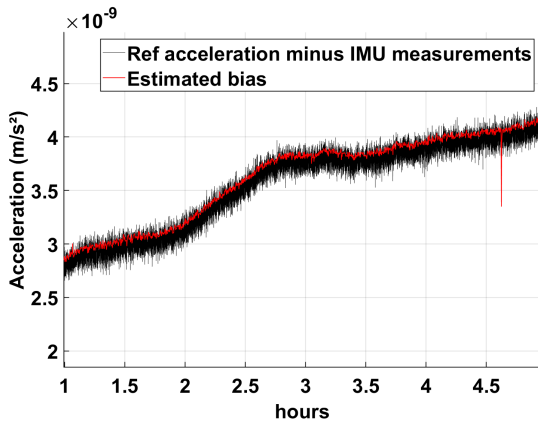actual observation in return to estimate the bias of the IMU bias.

Fig. 9: Recovery of the IMU bias using the measurements of the CAI accelerometer.

Figure 9 shows the recovery of the bias of the IMU in a satellite with hybrid accelerometer, in which the CAI reference mirror is connected to the IMU test mass. The assumption here is a perfect compensation of the rotational rates of the test mass. The more realistic case where we consider the full rotation effect in different scenarios will be a subject of future studies.

5. Conclusions

A GRACE-FO like satellite mission was simulated using the Hybrid Simulation Platform for Space Systems. Several non-gravitational forces were considered including solar radiation pressure, aerodynamic drag, Earth infrared pressure, albedo reradiation and thermal pressure. Furthermore, a separate test mass, acting as a reference mirror of a cold atom interferometer, was simulated inside the satellite. A mass-spring-damper system was utilized to model the connection between reference mirror and satellite. Through the coupling link, non-gravitational acceleration is transferred to the test mass. Real acceleration measurement data of GRACE-FO was used to check if the link spring and damping coefficients yield reasonable results. With the simulated acceleration data, the reference mirror position was calculated. Lastly, angular acceleration and velocity of the reference mirror were determined, showing that due to the coupling link, the reference mirror posses a angular velocity relative to the satellite.

We analyzed the accuracy of the measurements due to the movements, vibrations, misalignment and angular velocity of the test mass. Firstly, we showed that the translational acceleration of the test mass would not have a negative impact on the CAI measurements and the results would be very similar to the case where the CAI reference mirror is rigidly attached to the satellite body frame. We also showed that the angular velocity of the test mass hugely reduces the accuracy of CAI accelerometer, if no rotation compensation method is used. Therefore, we integrated a counter-rotating Raman wave vector across the interferometric sequence, which largely mitigated the Coriolis and centrifugal terms leading to an increased accuracy. We finally showed the possibility of having a hybrid accelerometer by using the test mass of a conventional accelerometer as the reference mirror of the CAI accelerometer and by combing the measurements using an Extended Kalman Filtering approach.

Going forward, controlling the reference mirror to compensate for the rotation with respect to the inertial frame, shows potential to reduce the phase shift error. Thus, developing a control system to steer the reference mirror and compensate for excess angular velocity will be attempted in the next test mass model.

Acknowledgement

References

[1] B. D. Tapley, S. Bettadpur, J. C. Ries, P. F. Thompson and M. M. Watkins. "GRACE Measurements of Mass Variability in the Earth System". In: *Science* 305.5683 (2004), pp. 503–505. DOI: 10.1126/science.1099192.

[2] R. P. Kornfeld, B. W. Arnold, M. A. Gross, N. T. Dahya et al. "GRACE-FO: The Gravity Recovery and Climate Experiment Follow-On Mission". In: *J Spacecr Rockets* 56.3 (2019), pp. 931–951. DOI: 10.2514/1.A34326.

[3] B. D. Tapley, M. M. Watkins, F. Flechtner, C. Reigber et al. "Contributions of GRACE to understanding climate change". In: *Nat Clim Change* 9.5 (2019), pp. 358–369. DOI: 10.1038/s41558-019-0456-2.

[4]   J. Chen, B. Tapley, C. Wilson, A. Cazenave et al. "Global Ocean Mass Change From GRACE and GRACE Follow–On and Altimeter and Argo Measurements". In: *Geophy Res Lett* 47.22 (2020). DOI: `10.1029/2020GL090656`.

[5]   K. Abich, A. Abramovici, B. Amparan, A. Baatzsch et al. "In-Orbit Performance of the GRACE Follow-on Laser Ranging Interferometer". In: *Phys Rev Lett* 123.3, 031101 (2019). DOI: `10.1103/PhysRevLett.123.031101`.

[6]   B. Christophe, D. Boulanger, B. Foulon, P.-A. Huynh et al. "A new generation of ultra-sensitive electrostatic accelerometers for GRACE Follow-on and towards the next generation gravity missions". In: *Acta Astronaut* 117 (2015), pp. 1–7. DOI: `10.1016/j.actaastro.2015.06.021`.

[7]   I. Daras and R. Pail. "Treatment of temporal aliasing effects in the context of next generation satellite gravimetry missions". In: *J Geophys Res: Solid Earth* 122.9 (2017), pp. 7343–7362. DOI: `10.1002/2017JB014250`.

[8]   R. Pail, R. Bingham, C. Braitenberg, H. Dobslaw et al. "Science and user needs for observing global mass transport to understand global change and to benefit society". In: *Surv Geophys* 36.6 (2015), pp. 743–772. DOI: `10.1007/s10712-015-9348-9`.

[9]   A. Trimeche, B. Battelier, D. Becker, A. Bertoldi et al. "Concept study and preliminary design of a cold atom interferometer for space gravity gradiometry". In: *Classical Quant Grav* 36.21, 215004 (2019). DOI: `10.1088/1361-6382/ab4548`.

[10]   F. Migliaccio, M. Reguzzoni, K. Batsukh, G. M. Tino et al. "MOCASS: A satellite mission concept using cold atom interferometry for measuring the Earth gravity field". In: *Surv Geophys* 40.5 (2019), pp. 1029–1053. DOI: `10.1007/s10712-019-09566-4`.

[11]   K. Douch, H. Wu, C. Schubert, J. Müller and F. Pereira dos Santos. "Simulation-based evaluation of a cold atom interferometry gradiometer concept for gravity field recovery". In: *Adv Space Res* 61.5 (2018), pp. 1307–1323. DOI: `10.1016/j.asr.2017.12.005`.

[12]   P. Abrykosov, R. Pail, T. Gruber, N. Zahzam et al. "Impact of a novel hybrid accelerometer on satellite gravimetry performance". In: *Adv Space Res* 63.10 (2019), pp. 3235–3248. DOI: `10.1016/j.asr.2019.01.034`.

[13]   A. HosseiniArani, B. Tennstedt, M. Schilling, A. Knabe et al. "Kalman-filter Based Hybridization of Classic and Cold Atom Interferometry Accelerometers for Future Satellite Gravity Missions". In: *Proceedings of the International Association of Geodesy Symposia, Beijing, China, June 28–July 2 2021*. Ed. by J. Freymüller and L. Sánchez. International Association of Geodesy Symposia. Accepted. Berlin, Heidelberg: Springer, 2022. DOI: `10.1007/1345_2022_172`.

[14]   S. Theil. "Satellite and Test Mass Dynamics Modeling and Observation for Drag-free Satellite Control of the STEP Mission". Dissertation. Bremen: Universität Bremen, 2002.

[15]   Barrett B., Gominet P.-A., Cantin E., Antoni-Micollier L. et al. "Mobile and remote inertial sensing with atom interferometers". In: *Atom Interferometry – Proceedings of the International School of Physics ´Enrico Fermi´*. Vol. 188. 2014, pp. 493–555. DOI: `10.3254/978-1-61499-448-0-493`.

[16]   M. Kasevich and S. Chu. "Measurement of the gravitational acceleration of an atom with a light-pulse atom interferometer". In: *Appl Phys B Photophys Laser Chem* 54.5 (1992), pp. 321–332. DOI: `10.1007/BF00325375`.

[17]   M. D. Lachmann, H. Ahlers, D. Becker, A. N. Dinkelaker et al. "Ultracold atom interferometry in space". In: *Nat Commun* 12.1, 1317 (2021). DOI: `10.1038/s41467-021-21628-z`.

[18]   S.-Y. Lan, P.-C. Kuan, B. Estey, P. Haslinger and H. Müller. "Influence of the Coriolis force in atom interferometry". In: *Phys Rev Lett* 108.9, 090402 (2012). DOI: `10.1103/PhysRevLett.108.090402`.

[19]   N. Zahzam, B. Christophe, V. Lebat, E. Hardy et al. "Hybrid electrostatic-atomic accelerometer for future space gravity missions". In: *Remote Sens* 14.14 (2022). DOI: `10.3390/rs14143273`.

[20]   A. Knabe, M. Schilling, H. Wu, A. Hosseini-Arani et al. "The Benefit of Accelerometers based on Cold Atom Interferometry for Future Satellite Gravity Missions". In: *Proceedings of the International Association of Geodesy Symposia, Beijing, China, June 28–July 2 2021*. Ed. by J. Freymüller and L. Sánchez. International Association of Geodesy Symposia. Berlin, Heidelberg: Springer, 2022. DOI: `10.1007/1345_2022_151`.

[21]   H. Y. Wen, G. Kruizinga, M. Paik, F. Landerer et al. *GRACE-FO Level-1 Data Product User Handbook*. Tech. rep. JPL D-56935 (URS270772). NASA Jet Propulsion Laborat-

ory California Institute of Technology, 2019. URL: https://podaac.jpl.nasa.gov/gravity/gracefo-documentation.

[22] R. Schwarz, S. Bremer, D. Seelbinder, M. List et al. "The Hybrid Simulation Platform for Space Systems (HPS): A Modular MATLAB/Simulink-Based Simulation Library for GNC Systems Development". In: *70th International Astronautical Congress (IAC), October 21–25, 2019, Washington, D.C., United States.* 2019. URL: https://elib.dlr.de/130466/.

[23] B. Bowman, W. K. Tobiska, F. Marcos, C. Huang et al. "A New Empirical Thermospheric Density Model JB2008 Using New Solar and Geomagnetic Indices". In: *AIAA/AAS Astrodynamics Specialist Conference and Exhibit, 18 August 2008 - 21 August 2008, Honolulu, Hawaii.* American Institute of Aeronautics and Astronautics, 2008. DOI: 10.2514/6.2008-6438.

[24] S. Behzadpour, T. Mayer-Gürr and S. Krauss. "GRACE Follow-On Accelerometer Data Recovery". In: *J Geophys Res: Solid Earth* 126.5, e2020JB021297 (2021). DOI: 10.1029/2020JB021297.

[25] C. M. McCullough, N. Harvey, T. Bandikova and H. Save. *Description of Calibrated GRACE-FO Accelerometer Data Products (ACT).* Tech. rep. JPL D-103863. NASA Jet Propulsion Laboratory California Institute of Technology, 2019. URL: https://podaac.jpl.nasa.gov/gravity/gracefo-documentation.

[26] C. Freier, M. Hauth, V. Schkolnik, B. Leykauf et al. "Mobile quantum gravity sensor with unprecedented stability". In: *J Phys: Conf Ser* 723,

012050 (2016). DOI: 10.1088/1742-6596/723/1/012050.

[27] K. Nicklaus, K. Voss, A. Feiri, M. Kaufer et al. "Towards NGGM: Laser Tracking Instrument for the Next Generation of Gravity Missions". In: *Remote Sens* 14.16, 4089 (2022). DOI: 10.3390/rs14164089.

[28] M. Misfeldt, V. Müller, L. Müller, H. Wegener and G. Heinzel. *Scale Factor Determination for the GRACE-Follow On Laser Ranging Interferometer including Thermal Correction.* 2022. DOI: 10.48550/ARXIV.2207.11470. arXiv: 2207.11470.

[29] S. Goswami, S. P. Francis, T. Bandikova and R. E. Spero. "Analysis of GRACE Follow-On Laser Ranging Interferometer Derived Inter-Satellite Pointing Angles". In: *IEEE Sens J* 21.17 (2021), pp. 19209–19221. DOI: 10.1109/JSEN.2021.3090790.

[30] B. Christophe, B. Foulon, F. Liorzou, V. Lebat et al. "Status of Development of the Future Accelerometers for Next Generation Gravity Missions". In: *International Symposium on Advancing Geodesy in a Changing World, International Association of Geodesy Symposia, Vol. 149.* Ed. by J. T. Freymueller and L. Sánchez. Vol. 149. International Association of Geodesy Symposia. 2018, pp. 85–89. DOI: 10.1007/1345_2018_42.

[31] B. Tennstedt and S. Schön. "Integration of atom interferometers and inertial measurement units to improve navigation performance". In: *28th Saint Petersburg International Conference on Integrated Navigation Systems (ICINS), 31.05.–02.06.2021, St. Petersburg, Russia.* Piscataway, NJ: IEEE, 2021. DOI: 10.23919/ICINS43216.2021.9470809.